Appl. Phys. B 66, 129–132 (1998)

Applied Physics B
Lasers
and Optics

Rapid communication

Simultaneous CH planar laser-induced fluorescence and particle imaging velocimetry in turbulent nonpremixed flames

C.D. Carter[1,*], J.M. Donbar[2], J.F. Driscoll[2]

[1] Innovative Scientific Solutions, Inc., 2786 Indian Ripple Rd., Dayton, OH 45440, USA
(E-mail: cartercd@possum.appl.wpafb.af.mil)
[2] University of Michigan, Department of Aerospace Engineering, Ann Arbor, MI 48109, USA

Received: 16 October 1997/Revised version: 30 October 1997

Abstract. We report the simultaneous measurement of the flamefront location, using single-shot CH planar laser-induced fluorescence (PLIF), and the velocity field, using two-color digital particle imaging velocimetry (PIV), in nonpremixed turbulent flames. To minimize the influence of particle scattering on the CH PLIF images, we pump a CH B-X(0,0) transition at 390 nm and detect A-X fluorescence at 420–440 nm, employing Schott glass filters to reject the strong particle scattering. The PIV images are recorded on a high-resolution (2036×3060 pixels) color CCD camera, and the velocities are derived from 64- or 128-pixel-square interrogation regions. We demonstrate this technique in a nonsooting, permanently blue nonpremixed turbulent jet flame ($Re_{\text{jet}} = 18\,600$). Here, PLIF images reveal a CH layer of thickness typically < 1 mm from flame base to tip. Furthermore, in these permanently blue flames, we observe instantaneous flamefront strain rates – derived from the PIV data – in excess of $\pm 10^4\ \text{s}^{-1}$ without flame extinction.

PACS: 07.60; 42.80; 82.40

Recently, combustion researchers have begun to apply simultaneous particle imaging velocimetry (PIV) and planar laser-induced fluorescence (PLIF) to study turbulent flames. Frank et al. [1] demonstrated the feasibility of PIV and PLIF imaging of biacetyl (as a marker of the reactants) in a premixed flame. Hasselbrink et al. [2] used simultaneous PIV and PLIF of the OH radical to investigate a nonpremixed CH_4-air flame. OH PLIF has the significant advantage of high signal strength, due to the abundance of superequilibrium OH near the flamefront; however, the use of high OH concentration as a marker of the primary reaction zone can be misleading. That is, persistence of the OH due to the slow three-body recombination reactions can indicate broad reaction zones, especially in the far field of jet diffusion flames. While these broad zones are indicative of regions of recombination reactions, they may not accurately mark the primary hydrocarbon reaction zone. While CH is effective at marking this layer of hydrocarbon reactions, it is usually found in very small concentrations (tens of ppm or less as compared to 10^3 to 10^4 ppm for OH); interfering fluorescence from polycyclic aromatic hydrocarbons (PAH), a soot precursor, further complicates single-shot planar imaging of CH. Nonetheless, under conditions where one can suppress soot formation without also suppressing CH formation, the coupling of PIV and CH PLIF is feasible. We have applied this combined technique to the study of 1) lifted, nonpremixed CH_4-air flames [3] – making measurements at the flame base, prior to the formation of PAH – and 2) nonsooting, permanently blue nonpremixed turbulent jet flames, where the fuel is diluted with N_2 and the oxidizer is pure O_2. In this communication, we illustrate this combined technique with measurements from a permanently blue flame.

For the CH PLIF, we tuned an Nd:YAG-pumped dye laser system to the $Q_1(7.5)$ transition of the $B^2\Sigma^- – X^2\Pi$ ($v' = 0$, $v'' = 0$) band ($\lambda = 390.30$ nm) and detected fluorescence from the A-X and B-X(0,1) bands, $\lambda = 420$–440 nm [4, 5]. Subsequent to laser excitation, the A state, $v' = 1$ and 0, is populated via fast electronic energy transfer (EET). Garland and Crosley [6] estimate a ratio of EET to B-state electronic quenching of 0.2; thus, the net fluorescence yield with this approach is significantly greater than that obtained by pumping an A-X(0,0) transition and detecting fluorescence from the A-X(0,1) band, where the ratio of the Einstein emission coefficients for the (0,1) and (0,0) bands is ~ 0.018 [7]. Because of the strength of the B-X(0,0) main-branch transitions [8], we observed strong saturation effects. While saturation has some benefits, e.g., reducing the dependence of the image on the laser-sheet irradiance distribution, it also has the disadvantage of increasing the apparent thickness of the laser sheet. Furthermore, at high laser irradiance, $\sim 2 \times 10^8\ \text{W/cm}^2$, a small but finite LIF signal was observed in the fuel core of a laminar nonpremixed flame. As the laser irradiance was decreased, the ratio of fuel-core signal to peak CH signal also decreased; as a consequence, we operated with a maximum probe-volume irradiance of $\sim 0.5 \times 10^8\ \text{W/cm}^2$ (15 mJ/pulse).

We generated the 390-nm laser radiation by wavelength mixing the output of a dye laser operating at 616.4 nm

* Corresponding author

with the residual 1064-nm radiation. The 390- and residual 616-nm beams were then separated, and the red beam was combined with a 532-nm beam from a second Nd:YAG laser. The beams were then formed into 35-mm-high sheets using a combination of one cylindrical and one spherical lens; before entering the test section, the red and green sheets were overlapped with the "blue" CH-excitation sheet. The FWHM of the CH beam was $\sim 200\,\mu$m; the two PIV beams were adjusted to have full widths of ~ 600–$800\,\mu$m at the probe volume, matching the PIV resolution for a 64-pixel-square interrogation region. The fields of view for the two cameras were matched at 24 mm (high) $\times$ 35.5 mm (wide). The delay between the two PIV beams was set with a digital delay generator and monitored with a photodiode and digital oscilloscope. The probe-volume beam energies for the PIV beams were set to ~ 15–20 mJ.

Using a fast Noct-Nikkor 58-mm $f/1.2$ lens, we collected and focused the CH fluorescence onto an intensified CCD array (Princeton Instruments); to improve the LIF signal strength, the CCD pixels were binned 2×2, resulting in an effective array size of 288×192 pixels. Of course, choice of appropriate filters is critical to recording the weak CH LIF signal and rejecting the strong scattering associated with PIV. In particular, Schott KV-418 and BG-1 (3-mm thick) filters provide excellent rejection of particle scattering at $\lambda = 390$ and 616 nm and good transmission, $\sim 65\%$, at 430 nm. Whereas the 390- and 616-nm beams are temporally coincident, the 532-nm beam from the second Nd:YAG laser is triggered $5\,\mu$s or more after the 30-ns gate of the LIF camera. The short intensifier gate reduced the influence of seed blackbody emission on the LIF images; nonetheless, with a several-second interval between exposures, dictated by the data-transfer time for the PIV camera, the LIF CCD accumulated significant charge due to the finite gate-off transmission of the intensifier. Thus, to mitigate this effect – and in the absence of a mechanical shutter – we used two trigger pulses. The first merely queued the PIV camera, while initiating image acquisition for the LIF camera and cleaning the CCD of this flame emission image; the second trigger pulse, initiated when the LIF camera completed data storage, caused both cameras to record an image.

The number density of the 0.5-μm Al_2O_3 seed particles was set at a level that provided a high percentage of good vectors and minimal interference to the CH images. PIV particle scattering from the 532- and 616-nm beams was recorded with a high-resolution (2036×3060 pixels, each $9\,\mu$m square) Kodak color CCD camera [9]. Digital two-color PIV has the following attributes: 1) directional ambiguity is resolved without the use of image-shifting techniques; 2) the particle displacement can be derived using cross correlations, which are superior to their auto-correlation counterparts [9]; 3) the image can be quickly processed (relative to film), which is a significant advantage when experimenting with optimum seed densities; and 4) resolution with the Kodak DCS 460 camera is comparable to that of the digitized 35-mm film image. To convert the particle scattering image to a velocity image, we employed the custom software package described by Gogineni et al. [9]. Note that the PIV camera was shuttered to 5 or 12.5 ms to reduce the influence of the particle blackbody emission; a custom trigger circuit synchronised the cameras' gate/shutter with the firing of the lasers.

A sample CH PLIF image from a permanently blue flame with the overlaid velocity vectors is shown in Fig. 1. The composite image was recorded at $z = 160$ mm from the fuel tube, corresponding to 0.67 of the stoichiometric flame length, L_f. Here, the fuel, composed of 30% CH_4 and 70% N_2 (by volume), issued from the 4.99-mm ID tube at ~ 70 m/s, resulting in a jet-exit Reynolds number of $Re = 18\,600$; the oxidizer was pure O_2 flowing at 0.3 m/s within the 150-mm-diameter coflow. In contrast to nonpremixed CH_4-air flames, these permanently blue flames stabilize just inside the shear layer. The concomitant large stoichiometric mixture fraction, $Z_{stoic} = 0.56$, combined with the heat release acts to retard the velocity decay such that the mean centerline velocity is ~ 58 m/s at $z/L_f = 0.67$. Figure 1 illustrates that the flamefront, as indicated by the CH image, is relatively thin, ~ 0.5 to 1.2 mm. This range of CH-layer thicknesses – more indicative of laminar flamelet-like reactions zones than thick distributed zones – is also representative of the values observed over many images at this downstream location. Note, however, that the smallest scales are presumably under-resolved as a result of the limited MTF of the camera/lens system.

The velocity vectors were resolved using 128-pixel-square interrogation regions (which were 75% overlapped), corresponding to 1.5-mm-square regions of physical space. The larger interrogation region (128- vs. 64-pixel-square) results in an increased signal-to-noise ratio and thus better accuracy for the velocities. With 128-pixel-square interrogation regions, the fraction of good vectors was typically $> 95\%$ (vs. $\sim 80\%$ with 64-pixel-square interrogation regions). Bad vectors were removed, and the surrounding good vectors were used to interpolate a new value. For the convenience of visualizing the local structures, i.e., vortices, 75% of the local mean centerline velocity, ~ 39 m/s at this downstream location, has been subtracted from all the vectors. Thus, the velocities on the low-speed oxidizer side appear as downward-pointing vectors. This figure reveals several structures acting to wrinkle, as well as thin or thicken the flamefront.

A subsection of Fig. 1 is shown in Fig. 2. Here, a vertical structure acts to pull a section of the flame in the positive radial direction. The corresponding strain rate vs. the tangential flame coordinate – i.e., the distance along the flamefront – is shown in Fig. 3. To compute the strain rate K_s, we use the relation for an axisymmetric flame [10]:

$$K_s = \frac{u_r}{r} + n_z^2 \frac{\partial u_r}{\partial r} + n_r^2 \frac{\partial u_z}{\partial z} - n_r n_z \left(\frac{\partial u_r}{\partial z} + \frac{\partial u_z}{\partial r} \right) . \qquad (1)$$

Here, r and z are the radial and axial coordinates, respectively, while u is the velocity and n is the flamefront normal. All partial derivatives were computed using standard central differences from the unfiltered, unsmoothed PIV velocity field. As noted above, the flame is stabilized just inside the shear layer where axial velocities can change rapidly over a small radial distance. Thus, under many circumstances the major contributor to large compressive/extensive strain is the $\partial u_z/\partial r$ term. Furthermore, large flamefront curvature can result in significant K_s, even with relatively small velocity changes.

Of course, we expect the instantaneous strain measurements to be somewhat noisy since we take derivatives of unfiltered PIV-derived velocities (although overlapping of interrogation regions does provide some smoothing). For example, a velocity error of ± 1 m/s (out of 60 m/s) between

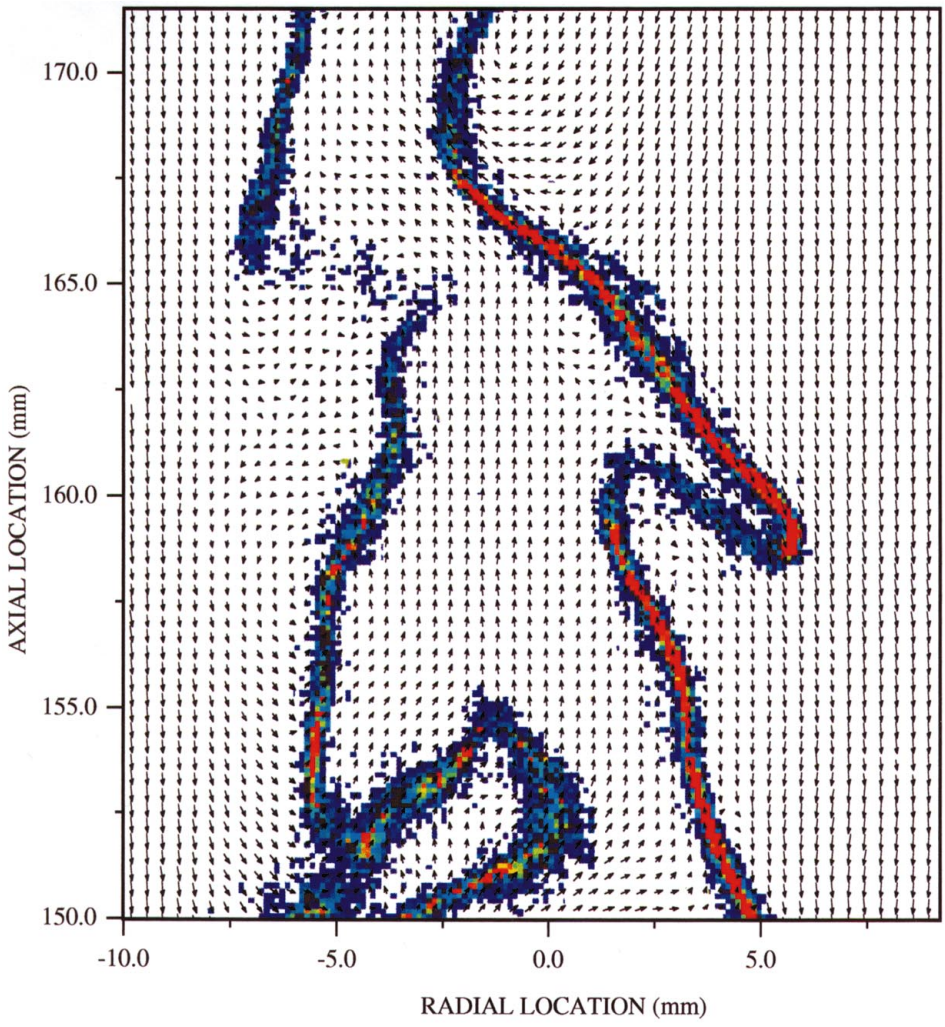

Fig. 1. CH fluorescence image with overlaid velocity vectors from a $Re = 18\,600$ flame. The respective downstream and radial coordinates are indicated on the ordinate and abscissa. Here, the PIV interrogation region is 1.5 mm square, and the regions are overlapped by 75%; also, 75% of the mean centerline velocity has been subtracted from all vectors

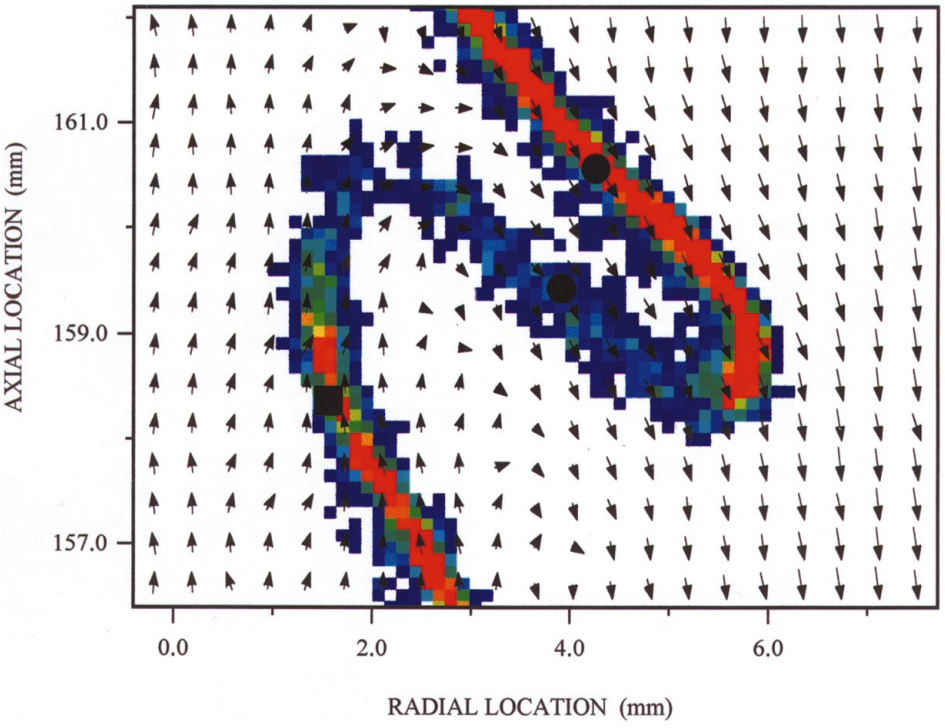

Fig. 2. Subsection of Fig. 1 from the region $r = -0.5$ to 9 mm and $z = 156$ to 162 mm

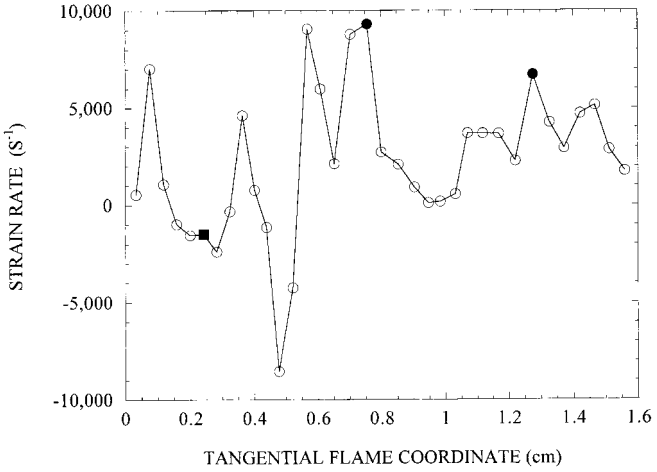

Fig. 3. Instantaneous flame strain rate vs. the tangential flame coordinate – i.e., the distance along the flamefront. For reference, the enclosed square and circles are indicated in both Figs. 2 and 3

adjacent interrogation regions (separated by 0.375 mm) results in an error of $2700\,s^{-1}$ in K_s. Nonetheless, the results from the measurements are clear: regions of large extensive and compressive strain exist within the flowfield. However, in this case, the flame has apparently not extinguished at the points of high strain, as is apparent from the CH PLIF images. Modeling calculations of steady counterflow diffusion flames (with the 30/70 mixture of CH_4 and N_2) show that with initially cold, unreacted fuel, the flame extinguishes at a strain of $\sim 10\,000\,s^{-1}$; with partially reacted fuel – more representative of the downstream conditions – the flame continues burning at strain rates as high as $30\,000\,s^{-1}$.

In summary, we report the combination of single-shot CH PLIF and PIV for the study of the effect of the flowfield on the flamefront in turbulent nonpremixed flames. We have demonstrated this technique in nonsooting, permanently blue jet flames. Within the permanently blue flames, we find that the CH layer – which can be highly contorted but rarely broken – remains thin, typically < 1 mm, from flame base to tip; furthermore, large compressive and extensive flamefront strain rates, $> 10^4\,s^{-1}$ in some regions, are observed without flame extinction.

Acknowledgements. This work has been supported by Wright Laboratory, Aero Propulsion and Power Directorate, Wright-Patterson Air Force Base, OH, under Contract Nos. F33615-92-C-2202 and F33615-97-C-2702, A.S. Nejad, Contract Monitor. JMD has received support from the USAF Palace Knight Program.

References

1. J.H. Frank, K.M. Lyons, M.B. Long: Combust. Flame **107**, 1 (1996)
2. E.F. Hasselbrink, M.G. Mungal, R.K. Hanson: AIAA Pap. 97-0118 (American Institute of Aeronautics and Astronautics, Washington, D.C. 1997)
3. K.M. Lyons, K.A. Watson, J.M. Donbar, C.D. Carter: "Scalar and velocity field measurements in a lifted CH_4-air flame", to be submitted for Combust. Flame
4. P.F. Bernath, C.R. Brazier, T. Olsen, R. Hailey, W.T.M.L. Fernando, C. Woods, J.L. Hardwick: J. Mol. Spectrosc. **147**, 16 (1991)
5. M. Zachwieja: J. Mol. Spectrosc. **170**, 285 (1995)
6. N.L. Garland, D.R. Crosley: Appl. Opt. **24**, 4229 (1985)
7. J. Luque, D.R. Crosley: J. Chem. Phys. **104**, 2146 (1996)
8. J. Luque, D.R. Crosley: J. Chem. Phys. **104**, 3907 (1996)
9. S. Gogineni, L. Goss, D. Pestian, R. Rivir: "High-resolution digital two-color PIV employing a single CCD camera", accepted for publication in Exp. Fluids
10. C.J. Mueller: *Measurements of Flame Vortex Interaction Dynamics and Chemistry* (Ph.D. Dissertation, Univ. of Michigan, Ann Arbor 1996)